Available online at www.sciencedirect.com
ScienceDirect
Journal of Power Sources 159 (2006) 301–306
JOURNAL OF POWER SOURCES
www.elsevier.com/locate/jpowsour

Short communication

The structure, lithium ion conductivity and reaction suppression against Li anode of the $LaAlO_3$–$La_{0.57}Li_{0.3}TiO_3$ solid solution

Kai-Yun Yang, Kuan-Zong Fung *

Department of Materials Science and Engineering, National Cheng Kung University, 1 Ta-Hsueh Road, Tainan 701, Taiwan

Available online 7 July 2006

Abstract

The structure, lithium ion conductivity and reaction suppression against lithium of the novel $xLaAlO_3$–$(1-x)La_{0.57}Li_{0.30}TiO_3$ oxides ($0 \le x \le 1$) with a perovskite related structure (ABO_3) are studied by using X-ray diffraction, ac impedance and digital multimeter. The results show that owing to the geometric environment, consisting of La^{3+}, Li^+ and vacancy at A-sites, the conductivities from $x = 0$ to 20 mol% are maintained in the range of 10^{-4} S cm^{-1}, and decrease to 8.92×10^{-9} S cm^{-1} with 30–40 mol% $LaAlO_3$ addition. When the value of x is larger than 50 mol%, the corresponding oxides no longer have the characteristic of ionic conduction. A stable solid electrolyte is also observed to alleviate the reaction significantly when the incorporated $LaAlO_3$ content is 40 mol%.

Keywords: Li^+ solid electrolyte; Reaction suppression; Structural screening

1. Introduction

Since the perovskite-type compound, $Li_xLn_{1/3}Nb_{1-x}Ti_xO_3$, was discovered by Latie et al. [1], a series perovskite-related compounds have continuously been studied with respect to their crystal structures and lithium ionic conductivity [2]. In particular, $La_{2/3-x}Li_{3x}\square_{1/3-2x}TiO_3$ (ABO_3, where $\square$ presents a vacancy, the La^{3+}, Li^+ and $\square$ are located at A-sites, and Ti^{4+} is at B-site.) received attention for its grain conductivity of 10^{-3} S cm^{-1} at 27 °C [2,3], and it has potential applications for use as the solid electrolyte of lithium battery.

Metallic lithium is the lightest and most electropositive metal to be the anode material to develop the smallest, high-power density and high-energy density battery. However, the lithium is so active that $La_{2/3-x}Li_{3x}TiO_3$ oxides may be unstable due to the contact with lithium. The reaction between them is suggested to include (1) the reduction of Ti^{4+} to Ti^{3+}, and (2) the Li^+ insertion into A-site vacancies [3]. The above conjectures can be indirectly proved by observing the increasing electronic conductivity. Because the instability results in the short-circuiting of the cell, this reaction needs to be suppressed, and this may be done by preventing at least one of the reaction processes from occurring.

This study will aim to decrease the Ti^{4+} concentration at the B-sites. Although a great amount of research has focused on the Ti cation substitution by Sn, Zr, Mn, Ge and so on [4], the process seemed unworkable due to the low solid solubility of these ions at B-sites. However, a novel solid solution ($LaAlO_3$–$La_{0.57}Li_{0.30}TiO_3$) was found by us as a probable solid electrolyte because $LaAlO_3$ with rhombohedral perovskite is expected to be more stable against lithium, based on the study of Hellstrom and Van Gool [5]. The first anti-reducible perovskite-type solid electrolyte is studied in the structure, electrical properties and reaction suppression against lithium.

2. Experimental

2.1. Sample preparation

The $La_{0.57}Li_{0.30}TiO_3$ (LLT) and $LaAlO_3$ (LA) powders were individually obtained by reacting stoichiometric amounts of La_2O_3 (purity 99.99%, Alfa, Ward Hill, USA), Al_2O_3 (purity 99.9%, Alfa, Ward Hill, USA), Li_2CO_3 (purity 99.4%, Alfa, Ward Hill, USA) and TiO_2 (purity > 99%, Strem, NEWBURYPORT, USA) at 1250 °C for 12 h. According to the respective ratio of x in xLA–$(1-x)$LLT with an interval of 10 mol%, these two reacted powders were mixed, pressed into discs, and sintered twice in air at 1350 and 1450 °C for 8 h, respectively.

* Corresponding author. Tel.: +886 6 2380208; fax: +886 6 2380208.
E-mail address: kzfung@mail.ncku.edu.tw (K.-Z. Fung).

0378-7753/$ – see front matter © 2006 Elsevier B.V. All rights reserved.
doi:10.1016/j.jpowsour.2006.04.117

In the sintering process, the samples were covered with the same composition powders to prevent the loss of the Li element. Subsequently, the samples were reduced in thickness by about 0.5 mm by surface grinder, and the final size was 4 mm in thickness and about 10 mm in diameter.

2.2. Analyses

The solid solubility and crystalline phase were analyzed using XRD with a Cu Kα radiation (λ = 1.5405 Å), and the XRD data were collected in the range from 10 to 90° (Model D-MAX III, Rigaku Co., Tokyo, Japan).

The electrical properties were measured in air by an A.C. Impedance method using a Solartron 1255B/1287 in a frequency range of 0.01–1 MHz and a temperatures range of 27–600 °C. The electrode for the measurement was prepared as follows. Pt paste was painted on both sides of the pellets and then, heated and held at 800 °C for 2 h as ohmic contact.

The phenomenon of reaction suppression was observed in Ar by an in situ method, utilizing a digital multimeter (Agilent 34970A) and lithium electrodes to measure the change in electrical conductivity. Before the measurement, the same thickness was required for the different samples evaluated. When Li electrodes contacted the sample, the resistances were simultaneously measured at 6-s intervals. Here, the thickness of the samples was 0.87 mm.

3. Results and discussion

3.1. Solid solubility and destruction of double perovskite

Fig. 1 shows the XRD patterns of solid solution $LaAlO_3$–$La_{0.57}Li_{0.30}TiO_3$. The complete solid solubility between LA and LLT is found. It can be discussed by the stability of the perovskite structure using the tolerance factor, t: $t = (r_A + r_O)/(\sqrt{2}(r_B + r_O))$, where r_A, r_B, and r_O are the respective ionic radii [6]. The stable perovskite structure is expected within the limits t = 0.88–1.09, using ionic radii based on coordination number (CN) 8 of B-site and CN 12 of A-site [7]. The calculated values for the LA–LLT are between 0.90 and 1.00. It promotes the formation of the solid solution, and indirectly proves that the Al^{3+} is located at the B-sites. By increasing the additional LA, the concentration of Ti^{4+} also decreases at B-site. Moreover, the shifting XRD peaks to the high-angle side reveal a decrease of average lattice parameter of perovskite unit cell with the addition of LA.

Fig. 1 also shows that LLT has a single phase with tetragonal perovskite structure resulting from an un-uniform distribution of La^{3+} ions among the sites 1a (0, 0, 0) (La1 layer: La^{3+}-rich) and 1b (0, 0, 1/2) (La2 layer: La^{3+}-poor) [8]. With LA addition, the intensities of the superlattice peaks decrease drastically at the composition of 10 mol% LA added compound. The ordered structure leads to the presence of the superlattice lines. Because of a lack of La^{3+} ions at the sites 1a (0, 0, 0), the Li^+ is expected to have high probability to hop via the La1 layer (two-dimensional transport mechanism: 2D). The structures, tending to disorder, reveal that La ions randomly distributed at A-sites. Therefore, the transport mechanism for Li^+ motion was changed from 2D to 3D.

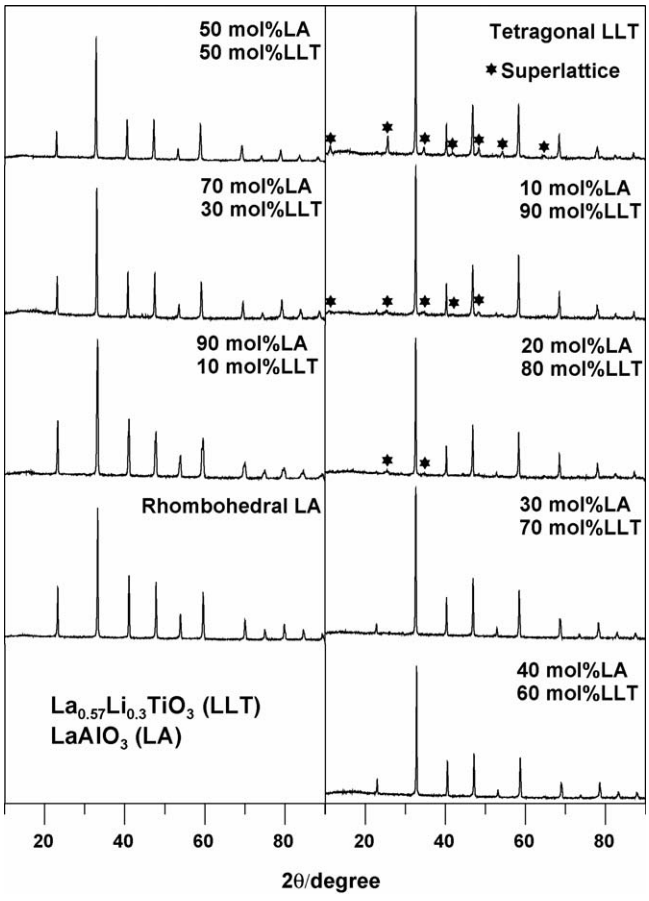

Fig. 1. X-ray diffraction patterns of solid solution $LaAlO_3$–$La_{0.57}Li_{0.30}TiO_3$.

3.2. Percolation limit on the occurrence of ionic conduction

Fig. 2 shows the impedance spectra of LA–LLT. According to the study of Inaguma et al. [3], the impedance spectrum of the polycrystalline 100 mol% LLT can be characterized as the ionic conductions of grain, and grain boundary in high- and low-frequency range, respectively. Furthermore, the blocking effect of the ionic charge carriers also occurs in the lower frequency range [9]. Therefore, the general equivalent circuit for the ionic conduction of LA–LLT can be expressed in Fig. 3. The conductive characteristics of grain and grain boundary contain the parallel resistance–capacitance contributions. When the LA addition was over 50 mol%, the ionic conduction feature disappeared even if these specimens were measured at high temperature. Rivera et al. [10] had indicated that the number of transport sites of the $Li_{0.5-x}Na_xLa_{0.5}TiO_3$ was controlled by the amount of Na and La obstacles, and the long-range dc conductivity value drastically decreased at x = 0.2, due to the percolative blocking of the 3D conduction network. Therefore, the percentage of the A-sites occupied by Li^+ or vacancy, that is, percolation/transport sites should be larger than the percolation threshold of the A-site simple cubic network [11], and then the structure could provide the skeleton of A-site network

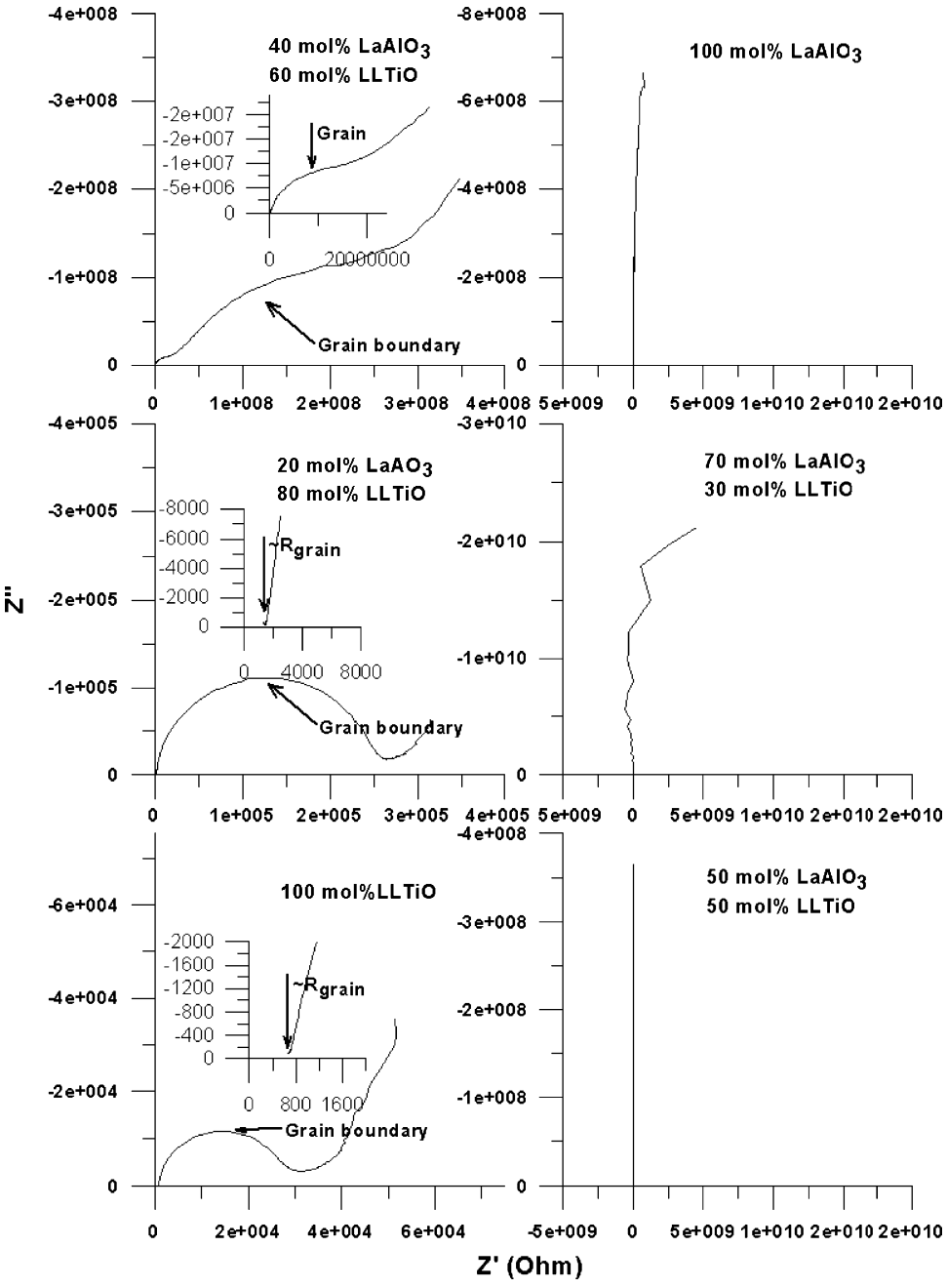

Fig. 2. The impedance spectra of solid solution $LaAlO_3$–$La_{0.57}Li_{0.30}TiO_3$ show the features of ionic conduction (high-frequency range: grain; low-frequency range: grain boundary; lower-frequency range: blocking effect of the ionic charge carriers).

for Li^+ transport. For LA–LLT, Table 1 shows that the concentration of the La obstacles increase with LA addition and the Li^+ conduction occurs when the total concentration of Li^+ and vacancies is larger than 0.26. Although Al^{3+} can completely substitute for Ti^{4+} in considering a stable solid electrolyte, not all LA–LLT compounds have Li^+ conductive ability. Only the 0–40 mol% LA added compounds have the percolation skeleton for Li^+ transport.

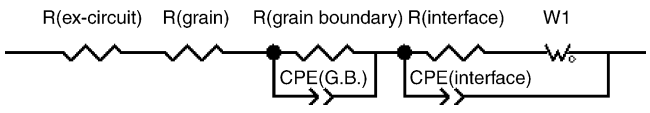

Fig. 3. The general equivalent circuit is used to describe the ionic conduction of $LaAlO_3$–$La_{0.57}Li_{0.30}TiO_3$.

3.3. The influence of $LaAlO_3$ addition on ionic conductivity

Table 1 lists the ionic conductivities of LA–LLT at 27 °C, and Fig. 4(a) shows this plotted against the LA addition, x. As can be seen, the conductivities of 0–20 mol% LA added LLT oxides maintain in the range of 10^{-4} S cm^{-1} and then the conductivities drastically decrease for other compounds. Such a change is ascribed to the following variations: the concentra-

Table 1
Li_A^+ and V_A'' concentrations, grain conductivity at 300 K, activation energy, and S index for the solid solution $xLa_{0.57}Li_{0.3}TiO_3$–$(1-x)$ $LaAlO_3$

x (mol%)	$[Li_A^+]$	$[V_A'']$	σ_g (S cm^{-1})	$E_{a,g}$ (kJ)	S
0	0.30	0.13	1.00×10^{-3}	3.42	1
10	0.27	0.12	7.93×10^{-4}	3.24	1.14
20	0.24	0.10	3.80×10^{-4}	3.47	0.59
30	0.21	0.09	1.81×10^{-5}	3.77	0.03
40	0.18	0.08	8.92×10^{-3}	3.96	$1.40 \times 10^{-}5$
50	0.15	0.07	0	–	0
60	0.12	0.05	0	–	0
70	0.09	0.04	0	–	0
80	0.06	0.03	0	–	0
90	0.03	0.01	0	–	0

tions of Li ions and vacancies, the ordered–disordered structure, the activation energy, and the skeleton of A-site network. These effects contributing to grain conductivity can be described in the equation [12]: $\sigma = (q^2r^2/kT)A[Li_A^+][V_A''] \exp(-E_a/kT)$, where r is the jumping distance of Li^+, A the geometry factor of structure, $[Li_A^+]$ Li^+ concentration, $[V_A'']$ A-site vacancy concentration, T absolute temperature and E_a is the activation energy for Li^+ hop.

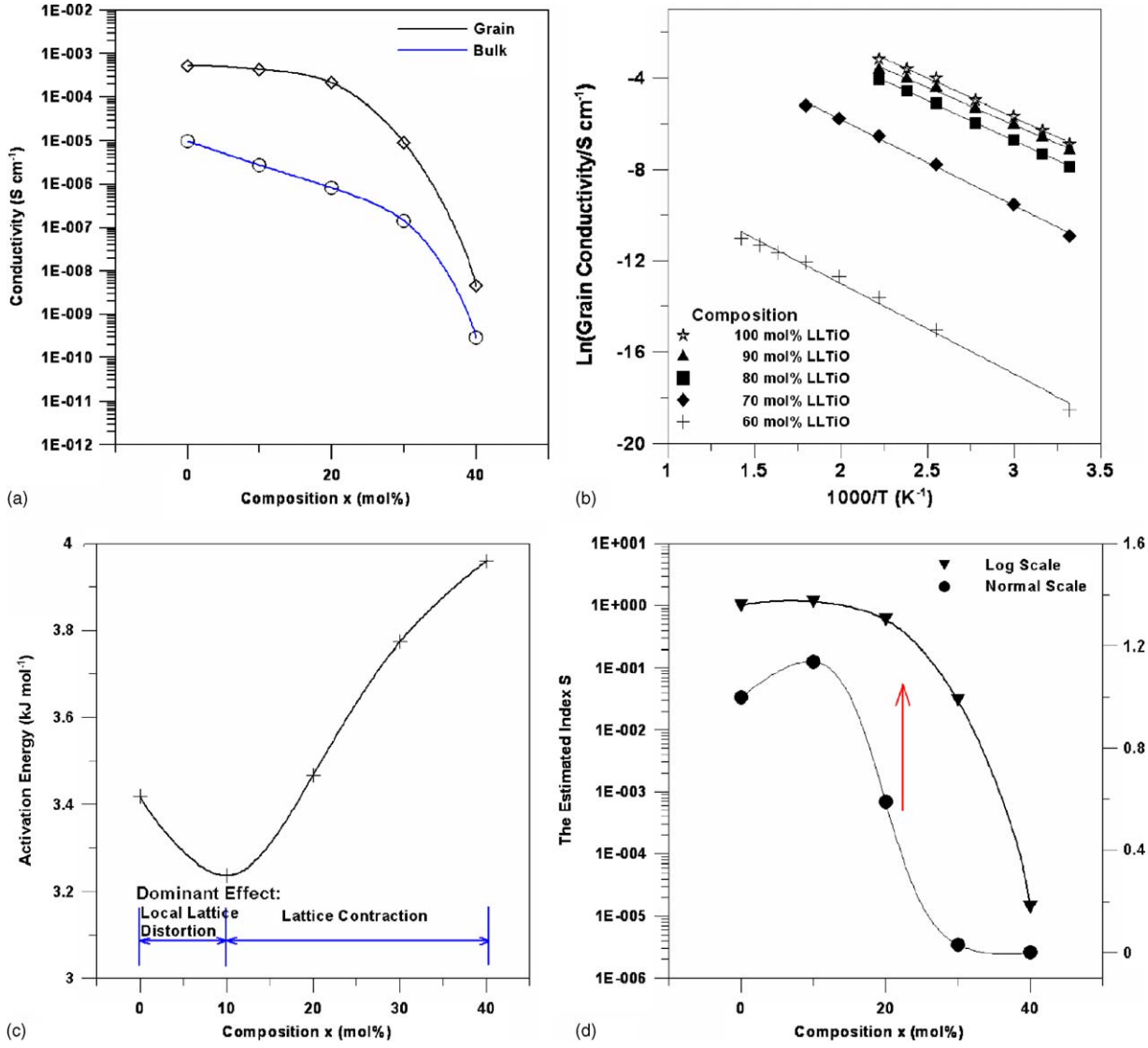

Fig. 4. The influences of $LaAlO_3$ addition (x in mol%) on ionic conductivity for solid solution $LaAlO_3$–$La_{0.57}Li_{0.30}TiO_3$: (a) the plots of grain and bulk ionic conductivity versus x at 27 °C; (b) Arrhenius plots of grain interior for different composition compounds, $xLaAlO_3$–$(1-x)La_{0.57}Li_{0.30}TiO_3$; (c) activation energy vs. x; (d) the estimated index S related to the ($LaAlO_3$–$La_{0.57}Li_{0.30}TiO_3$) geometry vs. LLTiO.

3.3.1. The influence of [Li_A^+] and [V_A''] on conductivity

Table 1 shows that both [Li_A^+] and [V_A''] decrease with LA addition. Although the decrease of [Li_A^+] and [V_A''] led to the decrease of conductivity, the charge carriers are still lithium ions. The role of the vacancies is the provider of percolation sites, which can also enhance Li^+ motion. Thus, the dominant effect on Li^+ conductivity is expected to be the Li^+ concentration.

3.3.2. The variation of activation energy

Activation energies for the ionic conduction were determined from Arrhenius plots as shown in Fig. 4(b). The results are summarized in Table 1 and shown as a function of the composition x in Fig. 4(c). The minimum value of 3.24 kJ is observed at $x = 10$ mol%. By raising the LA addition, the activation energies also increase. This is ascribed to the size of the Li^+ hopping channel, which relates to the average lattice parameter of perovskite unit cell. As mentioned in Section 3.1, the LA addition caused the decrease in the average lattice parameter. This seems to indicate the increase in activation energy due to contracting the size of the Li^+ hopping channel. However, an unexpected variation to the classical ionic crystal model was reported by Chung et al. [4] and Nakayama et al. [13], in that doping the different size cations with a small amount at B-sites would cause a local distortion of the lattice. The substituted cation with smaller size expands the size of the Li^+ hopping channel, and Li ions only require lower energy to overcome activation energy to move to an adjacent A-site vacancy. This local distortion effect on activation energy is also observed in Fig. 4(c). When larger LA amount of x is added, the Li^+ migration shows little relation to the local distorted lattice and is mainly determined by the classical ionic crystal model. Thus, the activation energy is raised.

3.3.3. The influences of the geometric environment of A-site network on conductivity

The ordered-disordered and Li^+ percolated/unpercolated structures changed by adding LA are classified as the geometric environment composed of Li^+, La^{3+} and vacancies at A-sites [14]. It can use the geometry factor A to express the contribution to ionic conductivity. In other words, the meanings of geometry factor can be used to describe whether the structure can provide the beneficial skeleton of A-site network for Li^+ motion. An index S will be made by us to comprehensively estimate these effects on conductivity as compared with the LLT structure. According to The Powder Diffraction Files, 87-0935 and 85-0848, the Li^+ jumping distance for LA–LLT is estimated in the range of 3.7–3.9 Å, and the value of $(r^2_{\mathrm{LLT-LA}}/r^2_{\mathrm{LLT}})$ is approximately one. The index S can be expressed as

$$S = (A_{\mathrm{LLT-LA}}/A_{\mathrm{LLT}}) = \frac{\sigma_{\mathrm{g,LLT-LA}}([\mathrm{Li}'_{\mathrm{A}}][V''_{\mathrm{A}}]\exp(E_{\mathrm{a}}))_{\mathrm{LLT}}}{\sigma_{\mathrm{g,LLT}}([\mathrm{Li}'_{\mathrm{A}}][V''_{\mathrm{A}}]\exp(E_{\mathrm{a}}))_{\mathrm{LLT-LA}}}.$$

Fig. 4(d) and Table 1 show the relation of S and LA addition. The S value increases before 10 mol% LA addition, and then it decreases drastically. There is a maximum value at $x = 10$ mol% LA. Harada et al. [15] had used XRD and quenched treatment to observe the ordered–disordered structure of LLT and concluded that fast ionic conduction was more favorable by decreasing the ordering extent of LLT. Herein, the tending disorder structure that results from less LA addition also creates the suitable geometric pathway for the faster Li^+ transport. Nevertheless, over-adding LA decreased the continuous transferring pathways in the structure due to more obstacles like La^{3+} at the A-sites. When the amount of percolation sites approaches the threshold, the amount of the localized blocking clusters drastically increases. Thus, the ionic conductivity decreases at the same time. This result reveals the mutual competition between the effects of order–disorder and decreasing percolation sites. The optimum geometry is observed at $x = 10$ mol% LA. In other words, this structure provides better a geometric environment than LLT for Li^+ motion, and when the LA addition was over 50 mol%, the geometry structure no longer provided any contribution to conductivity, that is, the value of S or A is equal to zero.

Considering the influences of Li^+ and vacancy concentrations, activation energy, and A-site structural geometry on ionic conductivity, the main effect from the structural geometry is shown in Fig. 4(a) and (d). Therefore, the conductivities of 0–20 mol% LA added compounds were maintained in the range of 10^{-4} S cm^{-1}, and with increasing LA addition, the conductivity decreased to 8.92×10^{-9} S cm^{-1}.

3.4. Reaction suppression against lithium

Fig. 5 shows the variation of the electrical conductivity of the solid solution using Li electrodes. It is found that all of the samples have the alteration process of ionic conduction to electronic conduction except for the 40 mol% LA added compound, and the resulting electronic conductivity, ascribed to the reduction of Ti^{4+}, also decreases with the Ti^{4+} substitution by Al ions. By increasing the LA addition, the conversion time is extended,

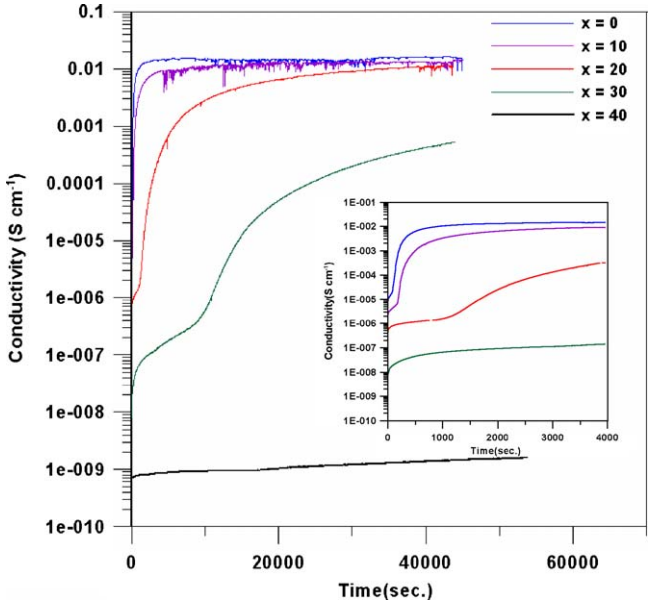

Fig. 5. The dynamic variation of the electrical conductivity plotted as a function of time for solid solution $x\mathrm{LaAlO_3}$–$(1-x)\mathrm{La_{0.57}Li_{0.30}TiO_3}$ with Li electrodes.

and this shows better inhibition. The reaction can be suppressed when the LA content is 40 mol%.

4. Conclusion

This work finds that the LLT and the selected LA can form a solid solution. Because the LA addition reduces the concentrations of Li^+ and vacancies in LA–LLT, only 0–40 mol% LA added compounds have the percolation skeleton for Li^+ transport. Over-adding LA causes the Li ions to be blocked in the localized blocking clusters so that the 50–100 mol% LA added compounds do not possess the Li^+ conduction features. Furthermore, the geometry related to the arrangement of A-site ions, like La^{3+}, Li^+ and vacancies, is the dominant factor to affect the ionic conductivity. Thus, the ionic conductivity is well maintained in the range of 10^{-4} S cm^{-1} for the 10–20 mol% LA added compounds. After adding 30–40 mol% LA, the increasing localized blocking clusters drastically decrease the ionic conductivity. Moreover, the reaction of the solid solution and lithium is suppressed when the LA content is 40 mol%.

Acknowledgments

The authors wish to thank the Nation Science Council of Taiwan for the financial support under contract No. NSC 92-2120-M-006-003 and 93-2120-M-006-004. Professors M.H. Hon and M.C. Wang kindly offer advice and suggestions on this work, for which we are very grateful.

References

[1] L. Latie, G. Villeneuve, D. Conte, G. Le Fiem, J. Solid State Chem. 51 (1984) 293.
[2] S. Stramare, V. Thangadurai, W. Weppner, Chem. Mater. 15 (2003) 3974.
[3] Y. Inaguma, C. Liquan, M. Itoh, T. Nakamura, Solid State Commun. 86 (1993) 689.
[4] H.T. Chung, J.G. Kim, H.G. Kim, Solid State Ionics 107 (1998) 153.
[5] E.E. Hellstrom, W. Van Gool, Revue Chim. Minérale 17 (1980) 263.
[6] V.M. Goldschmidt, Shrifter Norske Videnskop-Adad. Oslo, Matemot. Naturuid Klasse, 1926.
[7] O. Muller, R. Roy, The Major Ternary Structural Families, Springer-Verlag, New York, 1974, p. 221.
[8] A.D. Robertson, S. Garcia Martin, A. Coats, A.R. West, J. Mater. Chem. 5 (1995) 1405.
[9] J.T.S. Irvine, D.C. Sinclair, A.R. West, Adv. Mater. 2 (3) (1990) 138.
[10] A. Rivera, C. Leon, J. Santamaria, A. Varez, O. V'yunov, A.G. Belous, J.A. Alonso, J. Sanz, Chem. Mater. 14 (2002) 5148.
[11] M. Sahimi, Applications of Percolation Theory, Taylor and Francis, 1994, pp. 10–11.
[12] W.H. Flygare, R.A. Huggins, J. Phys. Chem. Solids 34 (1973) 1199.
[13] M. Nakayama, H. Ikuta, Y. Uchimoto, M. Wakihara, Appl. Phys. Lett. 81 (2002) 2977–2979.
[14] E.A. Secco, M.G. Usha, Solid State Ionics 68 (1994) 213–219.
[15] Y. Harada, Y. Hirakoso, H. Kawai, J. Kuwano, Solid State Ionics 121 (1999) 245.